# Sheffield Hallam University

# Comparative assessment of texture features for the identification of cancer in ultrasound images: a review

FAUST, Oliver <http://orcid.org/0000-0002-0352-6716>, ACHARYA, U Rajendra, MEIBURGER, Kristen M, MOLINARI, Filippo, KOH, Joel E W, YEONG, Chai Hong, KONGMEBHOL, Palin and NG, Kwan Hoong

**Citation:**

# Comparative assessment of texture features for the identification of cancer in ultrasound images: a review

Oliver Faust[a,*], U Rajendra Acharya[b,c,d], Kristen M. Meiburger[e], Filippo Molinari[e], Joel E W Koh[b], Chai Hong Yeong[d], Pailin Kongmebhol[f], Kwan Hoong Ng[d]

[a]*Department of Engineering and Mathematics, Sheffield Hallam University, United Kingdom*
[b]*Department of Electronic & Computer Engineering, Ngee Ann Polytechnic, Singapore*
[c]*Department of Biomedical Engineering, School of Science and Technology, Singapore University of Social Sciences, Singapore*
[d]*Department of Biomedical Imaging, Faculty of Medicine, University of Malaya, Kuala Lumpur, Malaysia*
[e]*Department of Electronics and Telecommunications, Politecnico di Torino, Turin, Italy*
[f]*Faculty of Medicine, Department of Radiology, Chiang Mai University, Thailand*

## Abstract

In this paper, we review the use of texture features for cancer detection in Ultrasound (US) images of breast, prostate, thyroid, ovaries and liver for Computer-Aided Diagnosis (CAD) systems. This paper shows that texture features are a valuable tool to extract diagnostically relevant information from US images. This information helps practitioners to discriminate normal from abnormal tissues. A drawback of some classes of texture features comes from their sensitivity to both changes in image resolution and grayscale levels. These limitations pose a considerable challenge to CAD systems, because the information content of a specific texture feature depends on the US imaging system and its setup. Our review shows that single classes of texture features are insufficient, if considered alone, to create robust CAD systems, which can help to solve practical problems, such as cancer screening. Therefore, we recommend that the CAD system design involves testing a wide range of texture features along with features obtained with other image processing methods. Having such a competitive testing phase helps the designer to select the best feature combination for a particular problem. This approach will lead to practical US based cancer detection systems which deliver real benefits to patients by improving the diagnosis accuracy while reducing health care cost.

*Keywords:* Cancer, Ultrasound, Texture Analysis, Computer Aided Diagnosis

## 1. Introduction

In 2015, heart diseases were the leading cause of death in the United States and cancer was the second leading cause of death. It is predicted that the order will reverse in the future [1]. Therefore, cancer is a big and growing public health problem [2]. Table 1 lists public health data from the American cancer society [3]. It shows both the estimated new cases and the estimated deaths for ovarian, liver, thyroid, breast and prostate cancers. These

---

*Corresponding author

Table 1: Estimation of the number of new cases and death for selected cancers in the United states, 2015 [3].

| Cancer type | Estimated new cases | Estimated deaths |
|---|---|---|
| Ovarian | 21,290 | 14,180 |
| Liver & intrahepatic bile duct | 35,660 | 24,550 |
| Thyroid | 62,450 | 1,950 |
| Breast | 234,190 | 4,0730 |
| Prostate | 220,800 | 2,7540 |
| All the cancer types from above together | 574390 | 108950 |
| All cancer types | 1658370 | 589430 |

cancers contribute 34.64% of all the estimated new cancer cases and they are responsible for more than 18.48% of cancer related deaths. In terms of public health, the problem can be partitioned into cancer prevention, diagnosis and treatment. Cancer prevention is possible, because healthy lifestyle choices lower the risk for developing cancer. The link between lifestyle choices and cancer was discovered by studies which showed that cancer rates of migrants move towards the rate measured in the indigenous population [4, 5]. Smoking, consumption of calorie dense food and reproductive behaviors are also known to increase the risk of getting cancer [4].

Ultrasound (US) is a non-invasive, cost effective and safe[1] medical imaging modality which can be used to detect cancer [6, 7]. Achieving a good diagnosis performance with this imaging technology requires an integrate interplay of fine motor skills (to operate the ultrasound transducer) and cognitive abilities for image interpretation [8]. Hence, practitioners require extensive initial training and continuous practice. A core problem of this human centric approach for disease diagnosis is the non-stationary diagnosis quality and inter- as well as intra-operator variability [9]. Non-stationary refers to the fact that the performance of human practitioners varies over time. These variations can be positive, such as gaining more experience over time as well as negative triggered by fatigue and other external factors. Overall, the beneficial properties of US technology outweigh these problems. Therefore, a vibrant research community explores a wide range of application areas for this imaging methodology. Initially, US was used only for application areas where tissue and bone formations led to sharp edges in the US images [10, 11]. Unfortunately, a wide range of diseases cannot be diagnosed based on the edges within an US image alone [12, 13]. Many of the new application areas target diseases whose symptoms and signs are changes in soft tissues [14]. A prominent example of that problem class is cancer diagnosis, because cancer cells are very similar to normal cells. Differentiating malignant from normal cells can be improved by interpreting image texture, since it contains information about the scanned tissues [15]. For a human practitioner, the changes in image texture, which indicate the presence of cancer, appear to be minute. Hence, human texture analysis is tiresome and error prone. As a consequence, a human centric approach leads to a low diagnostic accuracy.

Computer-Aided Diagnosis (CAD) can help to overcome the problems of human texture analysis and thereby increase the diagnosis accuracy [16, 17]. The challenge for such computer

---

[1]It uses no ionizing radiation.

based texture analysis is twofold. First, we need to establish mathematical definitions for relevant image textures. These mathematical definitions lead to texture analysis algorithms which can be used in practical CAD systems [18]. The second problem is to detect the texture changes, which indicate malignant tissues. It turns out that these problems cannot be solved a priori; the texture interpretation can only be done a posteriori. In other words, it is impossible to know what type of texture analysis algorithm will be sensitive for the subtle differences between normal and cancer cells in US images. Therefore, empirical methods identify which texture methods work well for a specific problem [19]. As a consequence, it is necessary to test a wide range of algorithms and select the ones which show the best performance on known data. Another complicating factor, for computer based texture analysis, is that most of the known texture algorithms depend on the image resolution. Hence, specific texture results are not transferable between different US capturing machines.

Texture information can be extracted using various methods. In order to select the best algorithm, it is necessary to have a good understanding of the available methods. The current review provides an overview of the available texture algorithms and their applications. We review texture-based US image analysis in the areas of breast, prostate, liver, ovarian and thyroid cancer detection. This review shows that texture features are vital for achieving the diagnostic accuracy needed for practical CAD systems. Furthermore, we give an overview of texture algorithms. During the review, we found that only a few CAD systems are solely based on texture methods. Research work, that considers only texture algorithms, aims to improve the understanding of the relationship between human tissue formations and US images. Robust and therefore practical CAD systems must be based on a range of different feature extraction methods, preferably coming from different imaging methods. We recognize that texture-based image analysis is a useful and cost effective enhancement of the well-known US technology. For application areas, such as breast, liver, ovarian, prostate and thyroid cancer, US based texture features are vital for CAD.

To support our position, on texture analysis for medical US images, we have organized the article as follows. The next section provides pathological background on breast, prostate, liver, ovarian and thyroid cancer and their typical characteristics in ultrasound images. The material section contains a comprehensive review of texture algorithms and we introduce methods to measure the quality of these algorithms. All studies that were cited in this review got informed consent from each study participant and protocol approval by an ethics committee or institutional review board. The review results section presents the review results for texture-based CAD for breast, prostate, liver, ovarian and thyroid cancer. The individual results are collected in tables, one for each disease. The subsequent discussion section puts these results into perspective with other works centered on CAD. The conclusion section ends the review with concluding thoughts on the topic of texture-based soft tissue cancer detection.

## 2. Background

In this section we will give an overview of prostate, ovarian, liver, breast and thyroid cancers and how US texture features are relevant for the identification of each individual cancer.
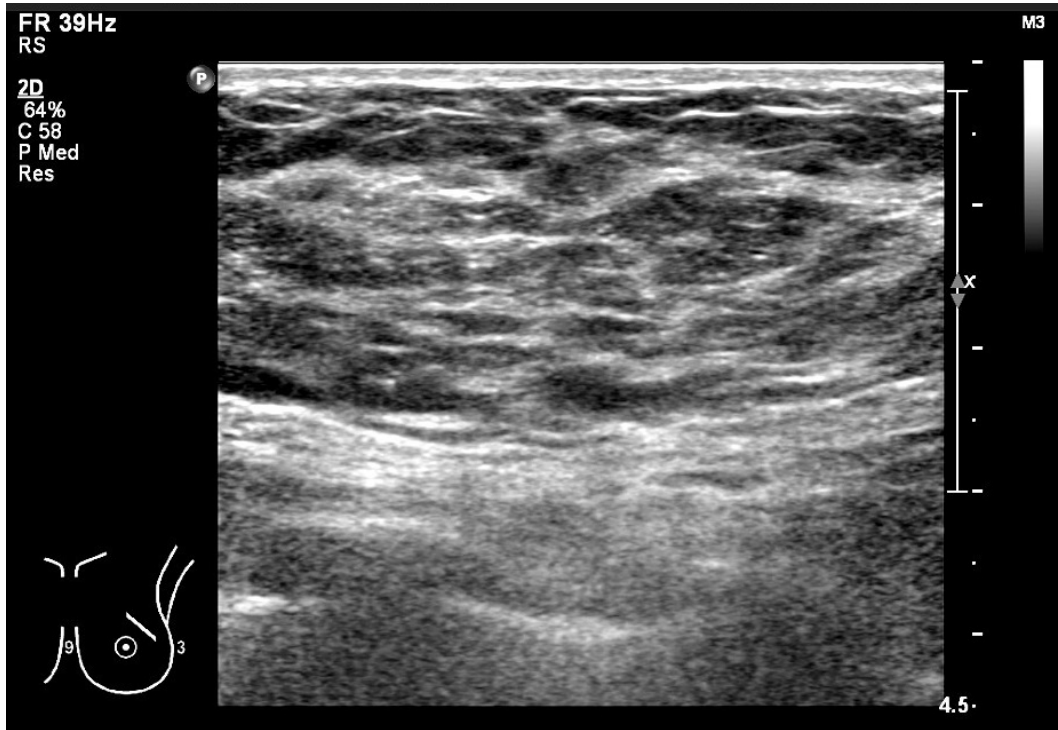
Figure 1: US image of a normal breast tissue.

### 2.1. Breast cancer

The female breast is made up of fat as well as connective and gland tissues, and its main biological purpose is to provide nutrients to newborns. Ultrasound imaging can be used to diagnose abnormalities in the breast and to distinguish between benign and malignant masses [20]. Breast tumors are visualized in the ultrasound image as a hypoechoic structure with a more or less circular form and malignant tumors often lack circumscribed margins, show heterogenous echo patterns and an increased anterioposterior dimension. Figure 1 shows a US image of normal female breast tissue. Figure 2 shows a benign cyst. Figure 3 shows a malignant carcinoma.

### 2.2. Prostate cancer

The prostate forms a part of the male reproductive system that secretes an alkaline fluid that constitutes about 30% of the semen volume [21]. Current methods used for screening for prostate cancer include measuring serum prostate-specific antigen (PSA) levels, transrectal ultrasound scanning (TRUS), digital rectal exam, and biopsy. Regarding ultrasound imaging, three dimensional TRUS is currently often used and abnormality in the US images can be determined by prostates that (1) have capsular irregularity or an ill-defined peripheral and transitional zone, or (2) are focal hypoechoic, echogenic or isoechoic with focal contour bulged lesions in the peripheral zone[22]. Figure 4 shows a US image of normal prostate tissue. Figure 5 shows suspicious prostate tissue which is calcified and enlarged.

### 2.3. Liver cancer

The liver is a vital organ for human health and well-being that filters toxic substances from the blood, synthesizes proteins and produces biochemicals for digestion [23]. Ultrasound
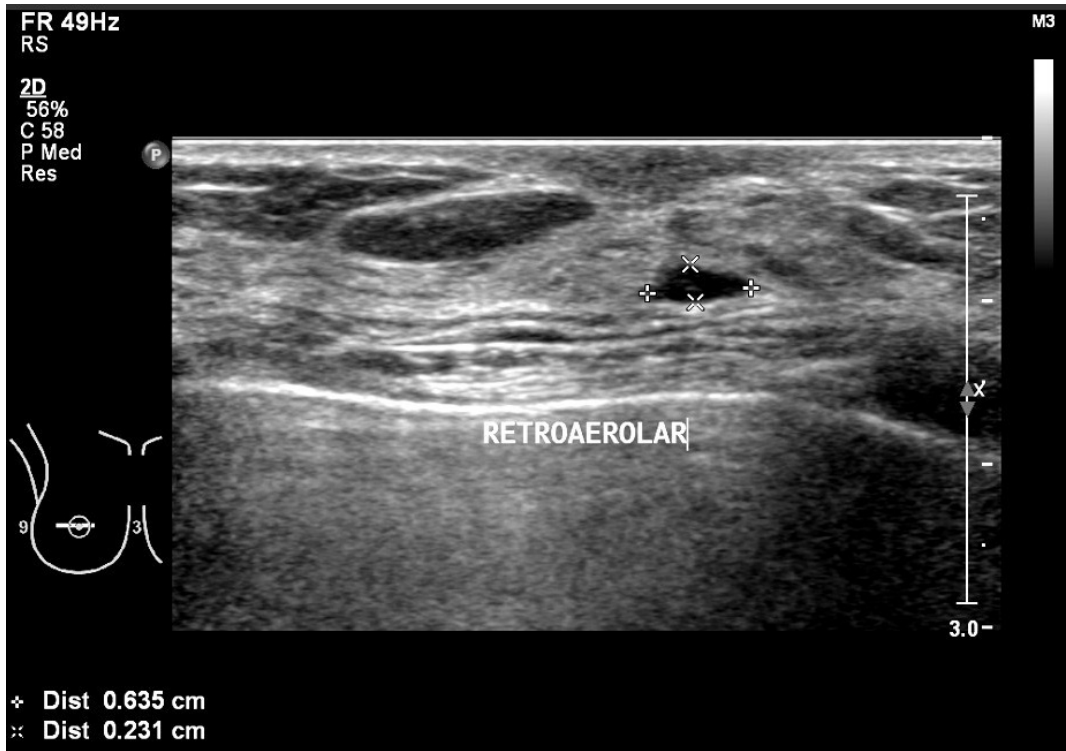
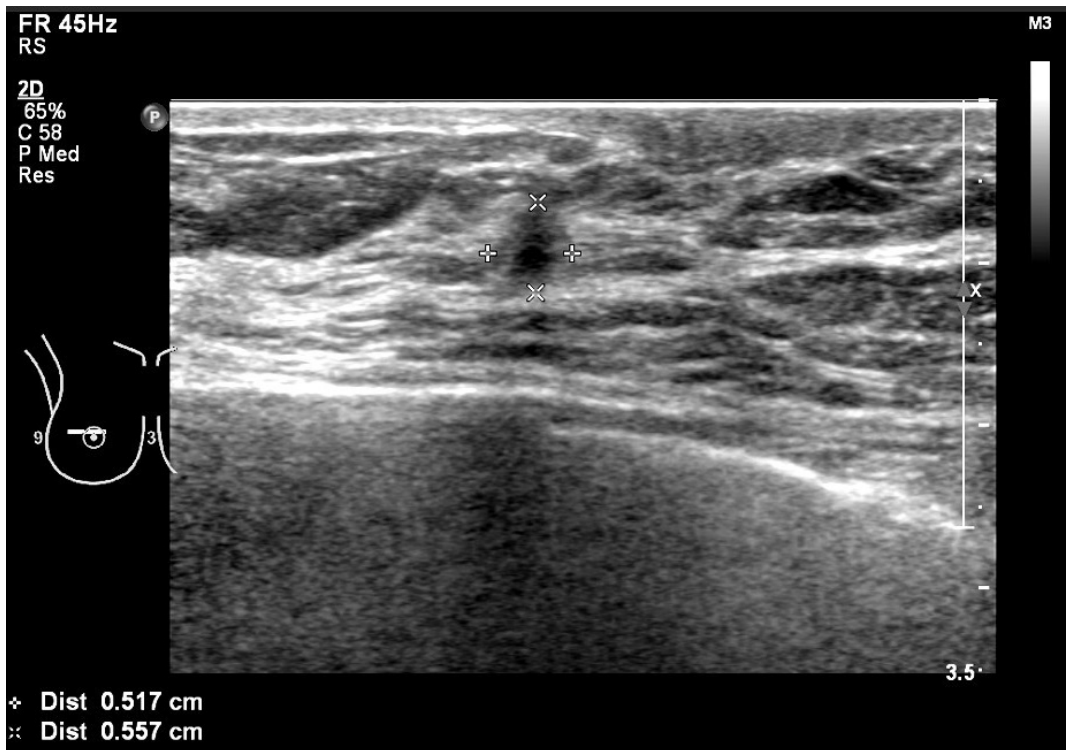Figure 2: US image of a benign breast cyst at the retroaerolar region.



Figure 3: Breast carcinoma: the lesion (measuring $0.517 \times 0.557$ cm) has a marked hypoechogenecity, lacks of circumscribed margins, shows heterogenous echo patterns and an increased anterioposterior dimension.

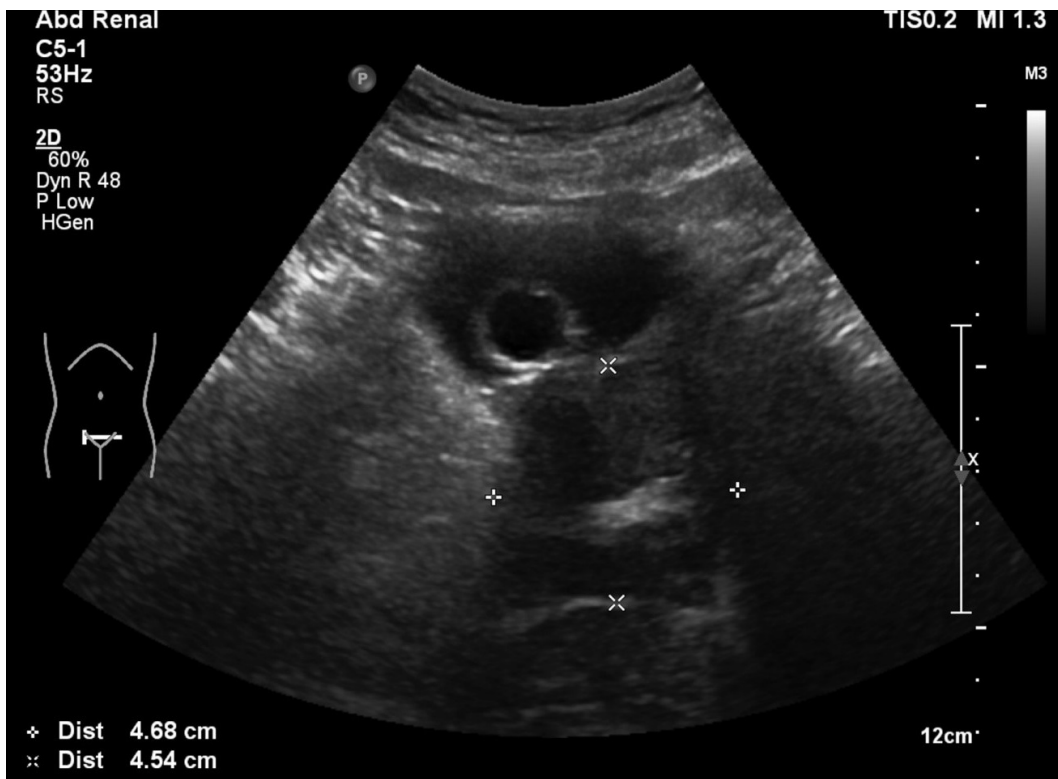Figure 4: US image of a normal prostate tissue.



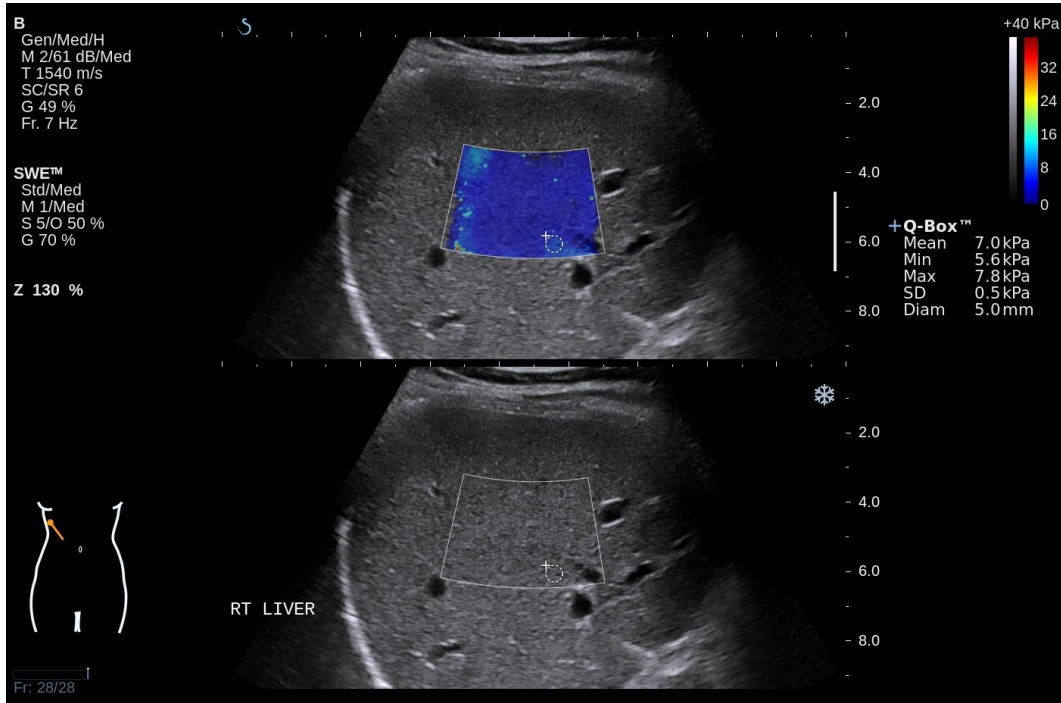Figure 5: US image of an enlarged prostate with calcification.

Figure 6: US images of a normal liver tissue. Top: Shearwave image. Bottom: B-mode ultrasound of the liver.

imaging is often used to diagnosis liver disease and in detecting lesions. A normal liver appears as a structure with homogeneous texture and average echogenicity, whereas cysts appear as an anechoic region with posterior acoustic enhancement and a typical metastasis presents a "target" appearance with a hyperechoic rim and a hypoechoic center [24]. Texture features can therefore be very useful in the diagnosis and discrimination of liver cancer. Figure 6 shows a US image of normal liver tissue. Figures 7 and 8 show US images of liver cyst and liver metastasis respectively.

## 2.4. Ovarian cancer

Ovaries are a part of the female reproductive system and are also responsible for producing female sex hormones, such as estrogen and progesterone [25]. Ultrasound imaging is often employed to image the ovaries and to assist in the detection and classification of ovarian cysts, which is a sac filled with liquid surrounded by a very thin wall. Ovarian cysts are typically classified based on size [26] and texture features can also enhance subtle tissue changes which indicate a malignant tumor. Figure 9 shows an US image of a normal ovary. Figure 10 shows an ovary cyst.

## 2.5. Thyroid cancer

The thyroid gland, which is located in front of the neck, secretes hormones that influence protein synthesis and the metabolic rate [27]. US imaging is often used to diagnose thyroid nodules which are typically characterized as hypo-, iso-, or hyperechoic [28]. Thyroid nodules are typically heterogeneous with various internal components, demonstrating how texture analysis can be a powerful tool in identifying cancer in thyroid US images. Figures 11 and 12 show benign and malignant thyroid respectively.
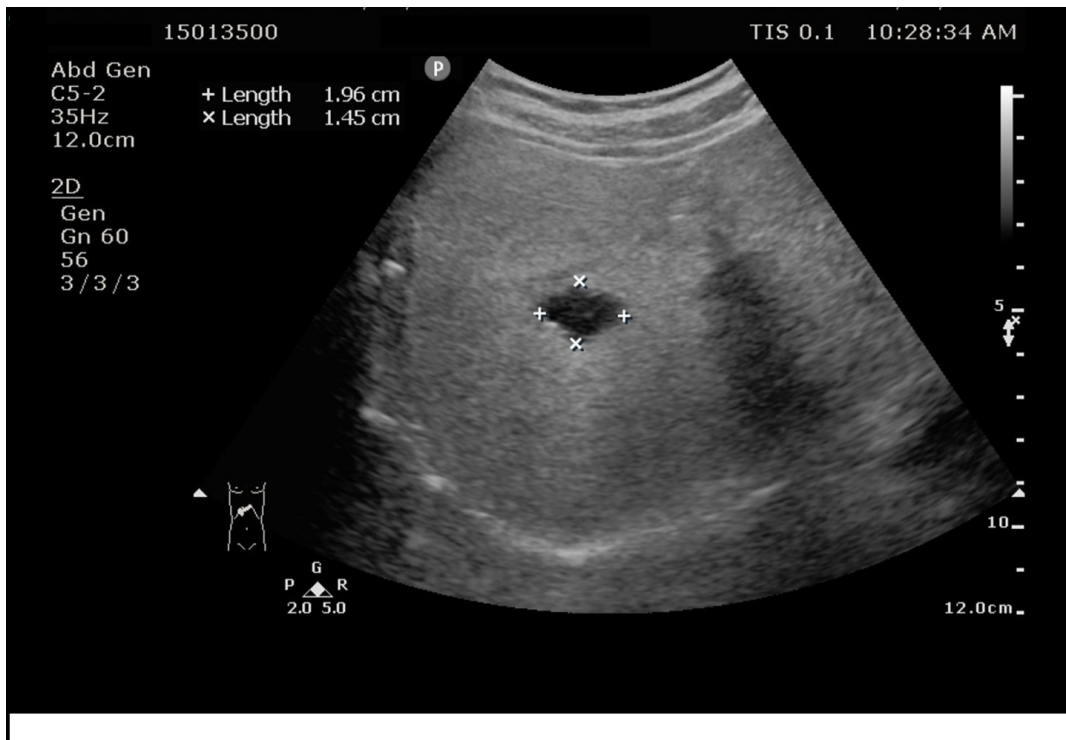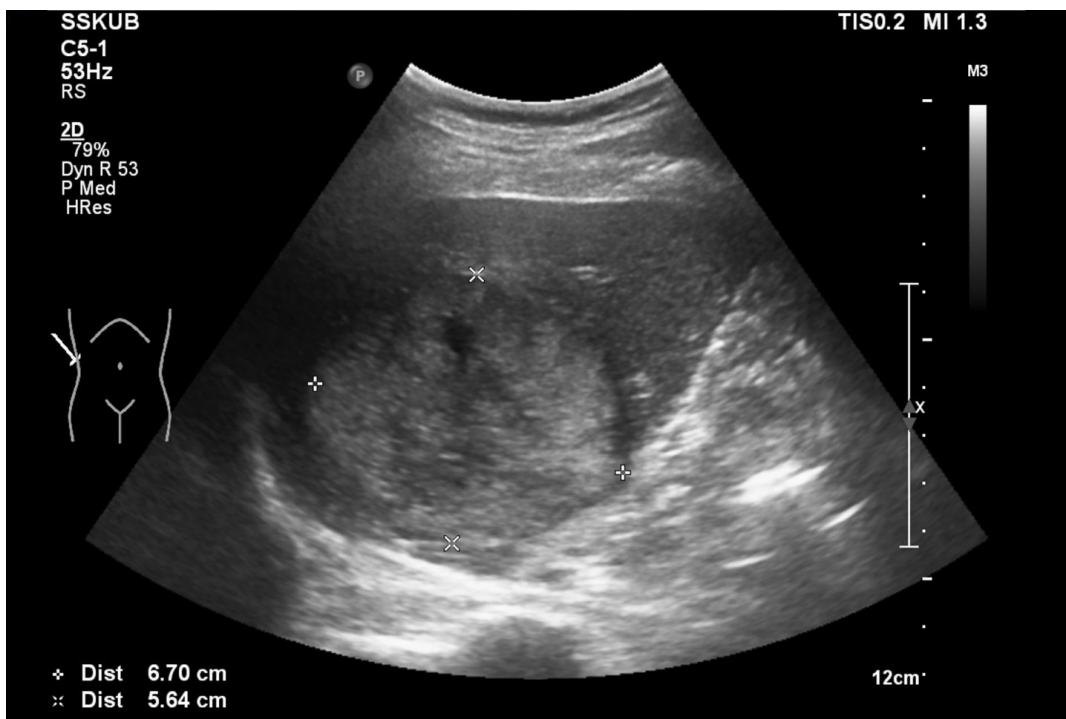
Figure 7: US image of a liver cyst.



Figure 8: US image of a liver metastasis.
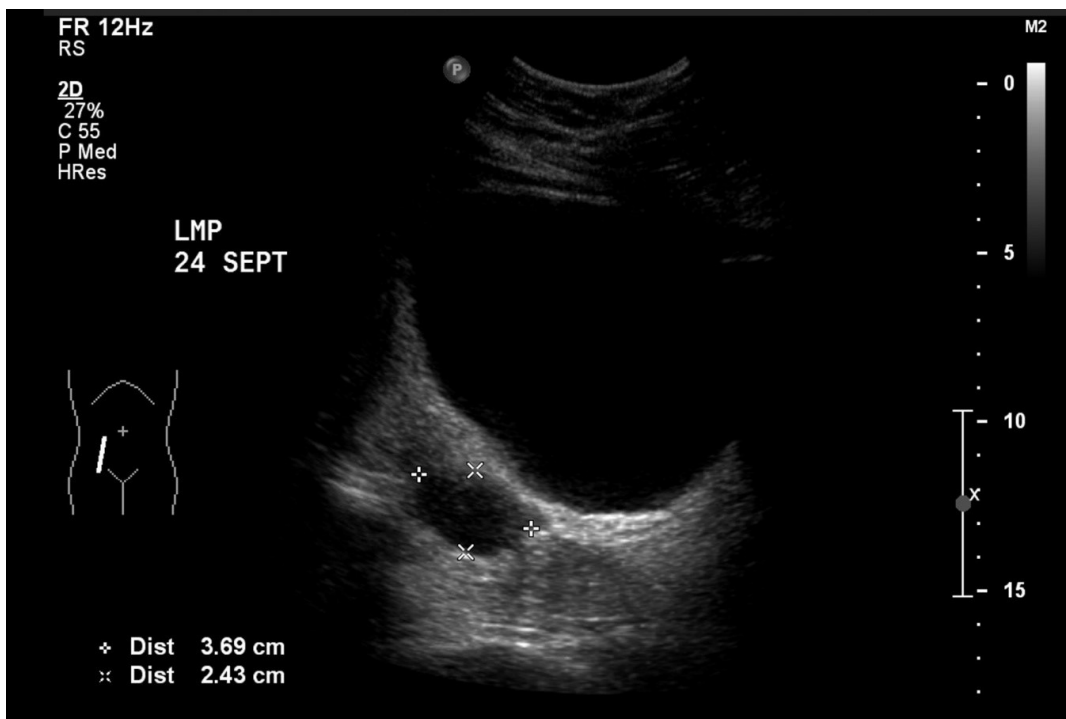
Figure 9: US image of a normal ovary tissue.



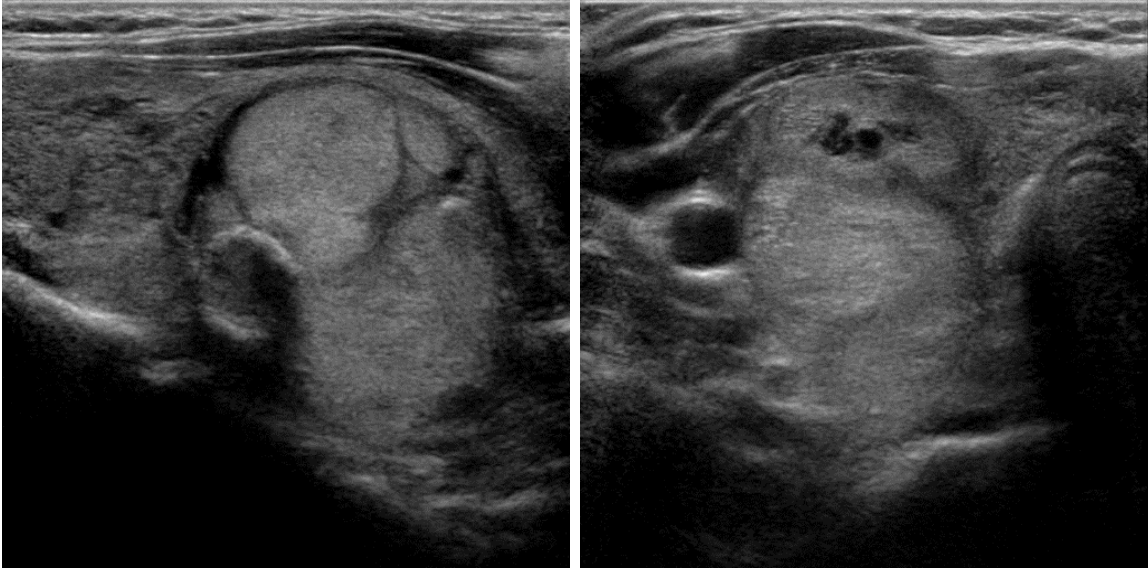Figure 10: US image of an ovary cyst.
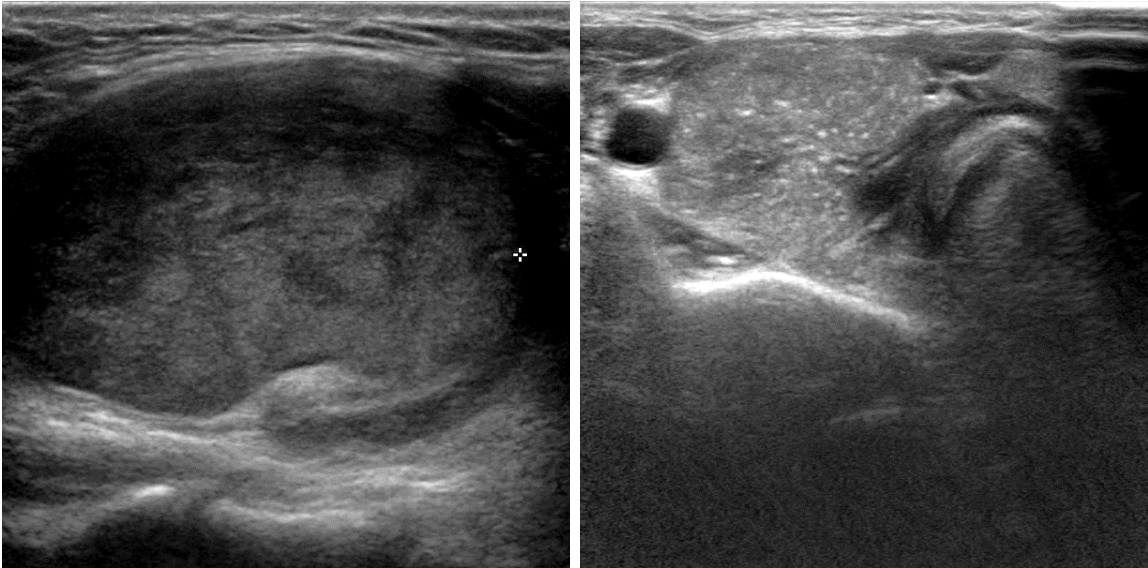
Figure 11: US images of a benign thyroid nodule.
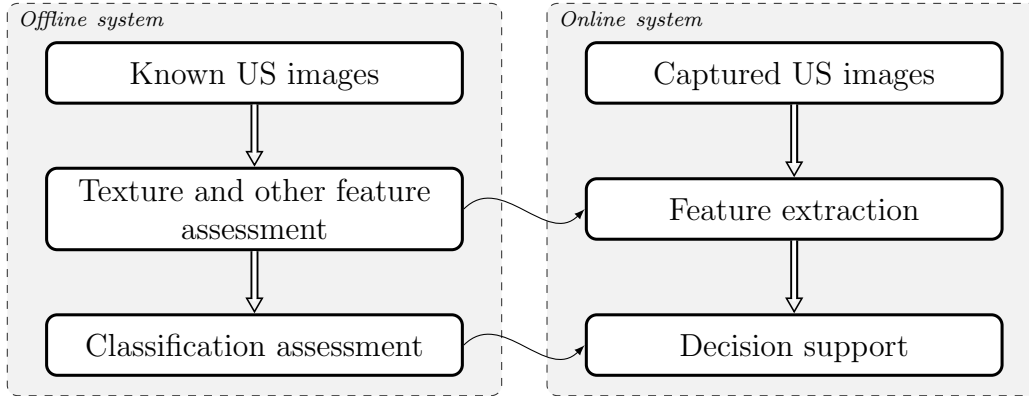


Figure 12: US images of a malignant thyroid.

Figure 13: The offline system is used to design the online or deployed CAD system.

## 3. Material and methods

The fact that cancer is a big and growing public health problem creates a need to investigate cost effective diagnosis methods. This section shows how US based CAD for soft tissue cancer can help to address this important problem. Cost efficiency comes from the fact that both US imaging and digital processing are inexpensive processes. The task of the designer is to find suitable image processing algorithms, which can extract good quality features from US images. These feature extraction algorithms feed their results to classification algorithms which provide diagnosis support.

Figure 13 shows an overview diagram for the design of US based CAD systems. The data set of known or classified US images is crucial for the validity of the design process. To be specific, only if the data set, with which the CAD system was developed, is similar to the measurements obtained when the system is deployed then the performance measures, acquired during the design process, are valid. The subsequent processing and classification methods are used to find the most suitable algorithm structure. This process is governed by empirical science and steered by performance measures. The next section introduces an example study on texture-based feature extraction from thyroid US images.

### 3.1. Ultrasound texture

US images show "speckle" texture, which results from the interaction of an ultrasonic wave with tissue components [29]. In many cases, parenthetical tissue structures are small compared to the period length of the sound waves used by the US transducer. As a consequence, the sound wave is scattered by these tissue structures. The scattered waves interfere with one another, because within one resolution cell there are several reflectors and the transducer sums up the received waves in a coherent manner. The interference produces a granular texture, known as speckle. The speckle pattern is influenced by a large number of parameters, including reflector density, tissue type and even the pathological state of the tissue [30]. All the scientific work reviewed in the next section is based on the assumption that speckle, i.e. the US image texture, contains information about the investigated tissue structure. More specifically, the reviewed work aims to differentiate speckle texture of benign from malignant tissue.

To demonstrate texture feature extraction, we used 60 texture algorithms on US images of the thyroid gland. The algorithms were applied to US scans from 223 patients of the Chiang Mai University Hospital, Thailand [31]. The protocol was approved by the ethics committee and the informed consent was waived due to retrospective study. The images show 211 benign and 31 malignant thyroid nodules. Figures 14 and 15 show the performance of these algorithms in differentiating benign from malignant tissue. The $t$-value [32, 7]was used as primary performance measure and the figures list the features in descending order, i.e. features with the highest $t$-values come on top of the list. Being on top of the list indicates that the feature has the ability to discriminate between benign and malignant thyroid nodules. In addition to the $t$-value, the figures also indicate mean and standard deviation scores, for both benign and malignant cases, of a particular feature. Ideally, we would like a feature to have distinct mean and low standard deviation values for benign and malignant lesions of US images. It turns out that the Long Run Emphasis ($LRE$) feature satisfies that requirement better than all the other tested texture algorithms. As a consequence, the $LRE$ $t$-value score is 3.4354, which is the highest amongst the tested feature extraction methods. However, this result holds true for this particular dataset only. Other datasets, taken with different imaging equipment, are likely to result in a different feature performance. Therefore, testing the feature performance with a large and varied dataset, is very important for the design of CAD systems.

Figure 16 shows a treemap [33] of the $t$-value results, presented in Table A.7, shown in the appendix. The Gray-Level Co-occurrence Matrix (GLCM) square shows the largest sub-squares, indicating that the method is sensitive for detecting malignant thyroid nodules.

The following classifiers were used for diagnosis support: Artificial Neural Network (ANN) [34], Support Vector Machine (SVM) [35], Decision Tree (DT) [36], Gaussian Mixture Model (GMM) [37], K-Nearest Neighbour (K-NN) [38], Probabilistic Neural Network (PNN) [39], Naive Bayes Classifier (NBC) [40], Self Organizing Feature Map (SOFM) [41], Multilayer Perceptron Neural Networks (MLPNN) [42], Radial Basis Probabilistic Neural Network (RBPNN) [43]. The next section reports the review results of a wide range of texture-based computer support systems used for cancer detection using US images.

## 4. Review results

The algorithms outlined above result from fundamental and applied research. In order for these algorithms to become technology, they have to work in more complex systems. In this section, we discuss how these algorithms were used in CAD systems. Each of the following sections presents the review results for texture-based CAD targeting a specific soft tissue cancer. We start the discussion by introducing the review results for breast cancer CAD.

### 4.1. Breast cancer

Table 2 summarizes research work, documented in eight papers, on texture methods for US based breast cancer detection. The table presents four different assessment criteria. The first assessment criterion is a list of all features used. We have placed a particular emphasis on texture algorithms. These algorithms are grouped in terms of GLCM, Gray Level Difference Matrix (GLDM), $LBP$, FOP and LTE. The next column states the number of features.
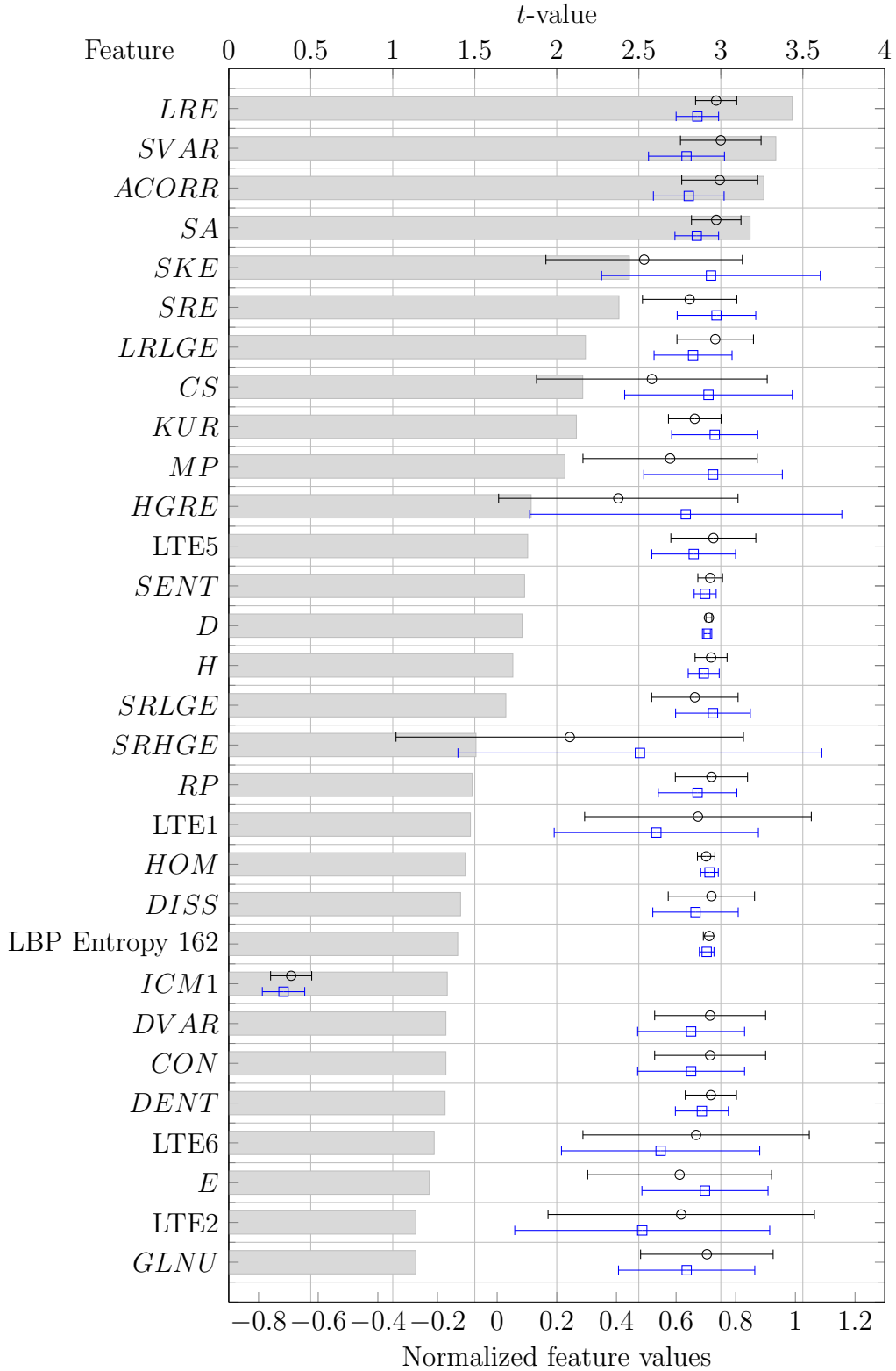
Figure 14: Error plot of normalized textrue features from US images of benign and malignant thyroid. The black error bar ⊢⊖⊣ indicates the feature mean and variance for features taken from images showing benign thyroid. Similarly, the blue error bar ⊢⊖⊣ indicates the feature mean and variance for features taken from images showing malignant thyroid. Both error bars are based on the normalized feature values. The length of the horizontal bar indicates the $t$-value.
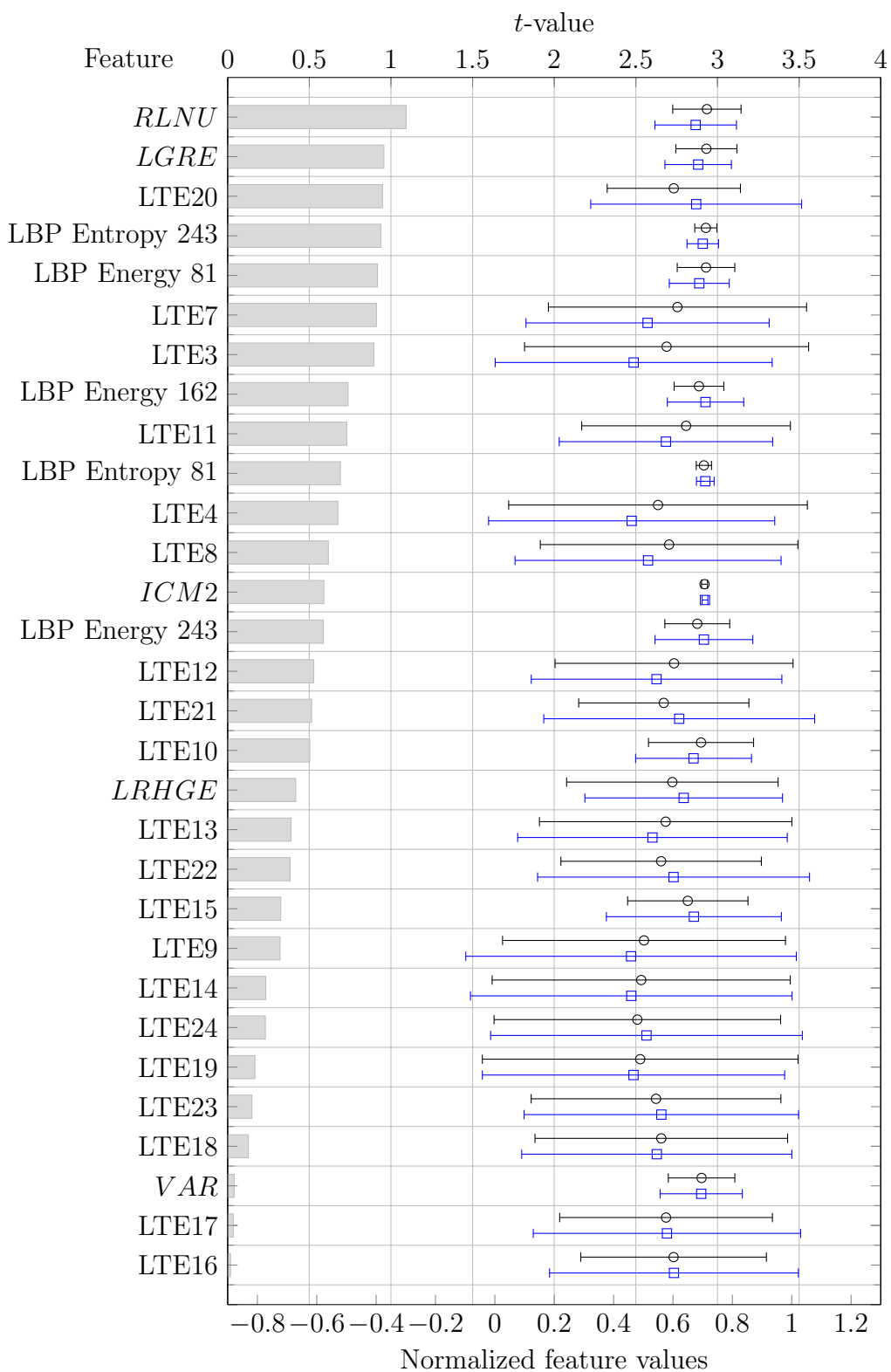
Figure 15: Error plot of normalized textrue features from US images of benign and malignant thyroid.
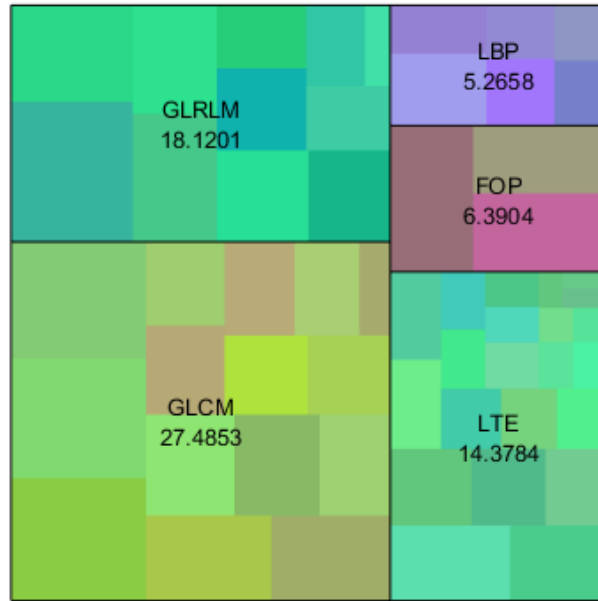
Figure 16: Treemap of the *t*-Value results presented in Table A.7 of Appendix Appendix A. The five main squares in the diagram represent the texture extraction methods GLCM, GLRLM, LTE, FOP and *LBP*. The number, below the square label, is the cumulative *t*-Value result of the texture extraction methods.

This number is an important assessment criterion, because it indicates the dimensionality of the feature vector which is fed into the classification algorithms. Column three states the classification algorithm used for the breast cancer CAD system. The last column indicates the performance of the best classification algorithm. As such, the classification performance gives an indication of the diagnostic quality that can be obtained with a specific system. However, the performance results need to be qualified with other assessment criteria in order to have a balanced assessment of the research work.

Table 2: Summary of breast cancer CAD using texture features in US images.

| Author year | Objective | Features | Number of Features | Classifiers | Performance and clinical significance |
|---|---|---|---|---|---|
| Huang et al. 2004 [44] | Detect the textural variation between benign and malignant tissues in US images for breast tumour classification. | Auto covariance of neighbouring pixels. | Principal Component Analysis (PCA) | Threshold classifier based on Euclidean distance | Accuracy >89.7%, Sensitivity >96.1 and Specificity >85.7%. |
| Huang et al. 2006 [45] | Establish an image retrieval technique that utilizes a projected principal vector to query US images, which have a similar texture, from a database. | • GLCM: Energy ($E$), Entropy ($H$), Correlation ($CORR$), Inertia ($IN$), Homogeneity ($HOM$)<br>• GLDM: Contrast ($CON$), Differential Mean ($DMEAN$), Difference Entropy ($DENT$), Inverse Difference Moment ($IDM$), Angular Second Moment ($ASM$) | After PCA: Feature vector dimensionality between 54 and 406 | Threshold | Accuracy: 82.38% |
| Huang et al. 2006 [46] | Benign and malignant breast tissue classification through texture features. | block difference of inverse probabilities (BDIP), block variation of local correlation coefficients (BVLC) and auto-covariance matrix | 28 | SVM | Accuracy: 95.2% |

| Chen et al. 2002 [47] | GLCM based tissue classification. | $CON$, Covariance ($COV$), Dissimilarity ($DISS$) | 32 | DT | Accuracy: 87.07%, Sensitivity: 95.35%, Specificity: 79.10% |
|---|---|---|---|---|---|
| Chang et al. 2003 [48] | Autocovariance coefficients of speckle textures for tissue classification. | Speckle autocovariance matrix | 24 | SVM | Accuracy: 93.2%, Sensitivity: 95.45%, Specificity: 91.43% |
| Garra et al. 2003 [49] | Texture analysis to improve the ability of ultrasound to distinguish benign from malignant nodules. | GLCM: Gray Scale Mean ($GSM$), Variance ($VAR$), Skewness ($SKE$), Run percentage ($RP$), $CON$, $ASM$, $H$, $CORR$, $LRE$, Relative frequency of edge elements, Variants of gradients, average absolute value of gradients. | 2 | Threshold | 100% sensitivity, specificity was 91% and accuracy was 93% |
| Shi et al. 2004 [50] | texture-based breast mass classification. | 151 Spatial Gray Level Dependence Matrices (SGLDM) features | 13 | Fuzzy SVM | Accuracy 74.71%, Sensitivity 88.89% and Specificity 64.71%. |

| Gómez et al. 2012 [51] | Sonographic texture analysis to distinguish malignant from benign breast lesions. | GLCM: Autocorrelation ($ACORR$), $CON$, $CORR1$,$CORR2$, Cluster Prominence ($CP$), Cluster Shade ($CS$), $DISS$, $E$, $H$, $HOM1$, $HOM2$, Maximum Probability ($MP$), Sum Average ($SA$), Sum Entropy ($SENT$), Sum Variances ($SVAR$), Difference Variance ($DVAR$), $DENT$, Information Correlation Measure 1 ($ICM1$), Information Correlation Measure 2 ($ICM2$), Inverse difference normalized, Inverse difference moment normalized. | 22 | Fisher Linear Discriminant Analysis (FLDA) | 87% accuracy |

## 4.2. Prostate cancer

Table 3 discuses seven works on prostate cancer using texture features in US images.

Table 3: Summary of prostate cancer CAD using texture features in US images.

| Author Year | Objective | Features | Number of Features | Classifiers | Performance |
|---|---|---|---|---|---|
| Scheipers et al. 2001 [52] | GLCM parameter for prostate tissue characterization. | • GLCM Details not specified<br><br>• Spectrum<br><br>• Parameters of an attenuation model | 16 | Fuzzy interference system | Accuracy 75% |
| Richard and Keen 1996 [53] | texture-based US prostate image segmentation. | LTE | Not discussed | Clustering | Not applicable for clustering |
| Mohamed et al. 2003 [54] | texture-based malignant mass detection. | Gabor filter texture segmentation. | Magnitude response and spatial smoothing | None | – |
| Basset et al. 1993 [55] | Detect tissue formations based on speckle texture. | GLCM: $ASM$, $CON$, $CORR$, $VAR$, inverse difference moment, $SA$, $SVAR$, $SENT$, $H$, $DENT$, Information measures of correlation, maximum probability | 12 | Threshold | Sensitivity: 83%, Specificity: 85% |
| Han et al. 2008 [56] | texture-based cancer pixel classification. | multiresolution autocorrelation. | Location, Shape | SVM | Accuracy 96.4% |
| Huynen et al. 1994 [57] | Malignancy detection based on spatial characteristics of image texture. | GLCM: Uniformity, $CON$, Inverse difference moment, $H$, $CORR$ | 5 | DT | Sensitivity 80,6%, Specificity 77.1% |

| Scheipers et al. 2003 [58] | texture-based cancer probability estimation. | • GLCM: $ASM$, $CON$, $CORR$, dimension, inverse difference moment, kappa, peak density, $VAR$, Signal to Noise Ratio (SNR) <br><br> • Spectrum | 28 | Fuzzy inference system | Accuracy 75% |
|---|---|---|---|---|---|

## 4.3. Liver cancer

Table 4 presents the automated diagnosis of fatty liver disease using texture features in US images. We have discussed six papers using texture features.

Table 4: Summary of liver cancer CAD using texture features in US images.

| Author year | Objective | Features | Number of Features | Classifiers | Performance |
|---|---|---|---|---|---|
| Pavlopoulos et al. 2000 [59] | texture-based detection of diffuse liver disease. | • FOP: Kurtosis ($KUR$), $VAR$<br>• Gray Level Run Length Statistics (RUNL): $RP$<br>• GLCM: $SENT$, $ASM$, $IDM$, $CON$<br>• Fractal Dimension Texture Analysis (FDTA): Hurst exponent ($Hurst$), Fractal Dimension ($D$) | 12 | Fuzzy neural network | Classification Accuracy: Normal: 80%, Fatty: 88%, Cirrhotic: 80% Overall accuracy of 82.67% in characterizing the different pathology |
| Poonguzhali and Ravindran, 2008 [60] | Detection of texture differences in focal lesions and normal tissue within the Region of Interest (ROI). | • GLCM: $SENT$, $H$<br>• GLRLM: $LRE$, Short Run Emphasis ($SRE$)<br>• Texture Enerrgy Measure (TEM): Spot ($S$), Level ($L$), Edge ($ED$)<br>• Gabor Wavelet | 8 | ANN | Correct classification: Normal liver lesion: 75%, cystic lesion: 94%, benign lesion: 81%, malignant lesion: 90% |

| Xian, 2010 [61] | Differentiation of malignant and benign liver tumours based on the idea that different tissues have different textures. | • GLCM: $SENT$, $CON$, $CORR$, $H$, $HOM$ | 5 | Fuzzy SVM | Dataset 1(DS1): accuracy: 97%, sensitivity: 100%, Specificity: 95.45%, Positive Predictive Value (PPV): 91.89% Dataset 2 (DS2): accuracy: 95.11%, sensitivity: 92%, Specificity: 95.5%, PPV: 85.19% |

| Acharya et al. 2012 [62] | Fatty liver detection based on the idea that the disease changes the liver tissue texture. | - GLCM: $HOM$, Texture Run Length percentage ($TexRL$)<br>- RUNL: $SRE$, Gray Level Non-Uniformity ($GLNU$)<br>- Higher Order Spectra (HOS)<br>- Discrete Wavelet Transform (DWT) | 3 ($SRE$, ePRes (12), DWT-Mean1sym4) | - DT<br>- Fuzzy classifier | All features, except the HOS feature, ePRes: Fuzzy (accuracy: 77.3%, PPV: 88.8%, sensitivity: 71.1%, specificity: 86.7%) All features except the DWT feature DWTMean1sym4: DT (accuracy: 93.3%, PPV: 100%, sensitivity: 88.9%, specificity: 100%) All features except the texture feature $SRE$: DT (accuracy: 93.3%, PPV: 100%, sensitivity: 88.9%, specificity: 100%) All features: DT (accuracy: 93.3%, PPV: 100%, sensitivity: 88.9%, specificity: 100%) |

| Singh et al. 2013 [63] | Fatty liver detection, based on the idea that an increase in the hepatocytes fat content results in a variation of the texture of liver surface. | <ul><li>GLCM $ASM$, $CON$, $CORR$, $VAR$, $IDM$, $H$, $SVAR$, $DVAR$, $DENT$, $H$ (two measures)</li><li>Gray Level Difference Statistics (GLDS), $HOM$, $CON$, $E$, $H$</li><li>FOP $GSM$ $SKE$ Kurtosis</li><li>TEM $L$, $ED$, $S$</li><li>Statistical Feature Matrix (SFM) Periodicity Roughness Coarseness Contrast</li><li>Frauenhofer Pattern Sampling (FPS) Radial sum Angular sum</li><li>Fuzzy Hurst exponent (two measures)</li></ul> | 7 | <ul><li>GLCM</li><li>Fuzzy neural network</li><li>SVM (Radial Basis Function (RBF) kernel)</li><li>Back propagation ANN</li><li>Fuzzy K-NN</li><li>Proposed fusing selected features using a linear classifier</li></ul> | The proposed method has an overall classification accuracy of 95% |

| Krishnan et al. 2013 [64] | Extracting diagnostically relevant texture information. | GLRLM: *SRE*, *LRE*, *GLNU*, Run Length Non-Uniformity (*RLNU*), *RP*, Low Gray-level Run Emphasis (*LGRE*), High Gray-level Emphasis (*HGRE*), Short Run Low Gray-level Emphasis (*SRLGE*), Short Run High Gray-level Emphasis (*SRHGE*), Long Run Low Gray-level Emphasis (*LRLGE*), Long Run High Gray-level Emphasis (*LRHGE*) | 11 | SVM | Disease Accuracy: Cirrhosis: 84.17%, Fatty: 92.50%, Hcc: 87.88%, Cyst: 100%, Hepatitis: 100% Overall Accuracy: 92.91% |
|---|---|---|---|---|---|
| Acharya et al. 2015 [7] | Fatty liver classification based on the fact that steatosis appears as a diffuse increase in echogenicity resulting from an increase in the parenchymal reflectivity. That increase results from the intracellular accumulation of fat-containing vacuoles. | GLRLM, *LBP* | Not reported | ANN, SVM, K-NN, DT, NBC | Not reported |

| Acharya et al. 2016 [65] | Detecting fatty change based on US texture. | GLRLM, GLRLS, LTE | 7 | DT, SVM, PNN, K-NN, linear discriminant analysis, quadrature discriminant analysis, NBC | Accuracy: 97.33%, specificity: 100.00% and sensitivity: 96.00% |
|---|---|---|---|---|---|
| Acharya et al. 2016 [66] | Texture methods to characterize and classify the normal and abnormal liver tissues. | GIST descriptors | Clinically significant features | DT, SVM, AdaBoost, K-NN, PNN, NBC | With PNN: Accuracy: 98%, specificity: 100.00% and sensitivity: 96.00% |

## 4.4. Ovarian cancer

Table 5 details research work on ovarian cancer using texture features in US images. The four papers discuss the use of texture features to extract diagnostically relevant information from US images of the ovaries.

Table 5: Summary of ovarian cancer CAD using texture features in US images.

| Author year | Objective | Features | Number of Features | Classifiers | Performance |
|---|---|---|---|---|---|
| Acharya et al. 2013 [67] | Correlation between tumor type and lesion diameter. The lesion diameter manifests itself as non-linear texture changes. | • Deviation, Fractal Dimension (FD) <br> • GLCM: $H$, Moment $(m_x)$ with $x = 4$ <br> • GLRLM: $RLNU$, <br> • HOS | 4 | DT | Accuracy: 97%, Sensitivity: 94.3%, Specificity: 99.7%, PPV: 99.7% |
| Acharya et al. 2013 [68] | texture-based tumor classification. | • $LBP$ <br> • LTE | 16 | SVM with: Linear, Polynomial order 1,2,3, and RBF kernel | SVM with RBF kernel: Accuracy: 99.9%, Sensitivity: 100%, Specificity: 99.8%, PPV: 99.8% |

| Acharya et al. 2014 [69] | texture-based tumor detection. | • FOP: Mean ($MEA$), $KUR$, $VAR$<br><br>• GLCM: $CON$, $ACORR$, $MP$, $DISS$, $HOM$, $E$, $CORR$, $CS$, $VAR$, $SA$, $SENT$, $SVAR$, $DVAR$, $DENT$, $H$ (Two measures)<br><br>• GLRLM: $SRE$, $LRE$, $GLNU$, $RLNU$, $RP$, $LGRE$, $HGRE$, $SRLGE$, $SRHGE$, $LRLGE$, $LRHGE$ | 11 | • PNN<br>• SVM<br>• DT<br>• K-NN | Detect ovarian tumor with 100% classification accuracy, sensitivity, specificity, and positive predictive value |
| Khazendar et al. 2015 [70] | texture-based detection of ovarian masses. | $LBP$ | 187 | • SVM<br>• K-NN | Performance significantly improved to an average accuracy of 0.77 (95% CI: 0.75-0.79) when images were pre-processed, enhanced and treated with a Local Binary Pattern operator (mean difference 0.15: 95% 0.11-0.19, p < 0.0001, two-tailed t test). |

| Acharya et al. 2015 [71] | Using texture to detect the subtle tissue changes which indicate a malignant tumor. | $LBP$, LTE | DT, Fuzzy Sugeno, K-NN, PNN, SVM | Not reported | Not reported |

### 4.5. Thyroid cancer

Table 6 introduces work on US based thyroid cancer detection. The six articles focus on texture-based features to discriminate between normal and malignant thyroid nodules.

Table 6: Summary of thyroid cancer CAD using texture features in US images.

| Author year | Objective | Features | Number of Features | Classifiers | Performance |
| --- | --- | --- | --- | --- | --- |

| Chang et al. 2010 [72] | texture-based thyroid nodule classification. | • GLCM: $CORR$, $DENT$, $DVAR$, $SA$, $SENT$, Sum of Squares ($SoS$), $SVAR$, $CON$, $E$, $H$, $HOM$, $CS$, $CP$ <br>• Statistical feature matrix <br>• GLRLM: $SRE$, $LRE$, $GLNU$, $RLNU$, $RP$ <br>• LTE <br>• Neighboring grey level dependence matrix, <br>• DWT, <br>• Fourier feature based on local Fourier coefficients. | 78 (13 GLCM, 1 Statistical feature matrix, 5 GLRLM, 10 LTE, 5 Neighboring grey level dependence matrix, 12 DWT, 32 Fourier feature based on local Fourier coefficients. | • SVM <br>• MLPNN <br>• PCA network <br>• RBF network <br>• SOFM network | SVM has the highest accuracy of 100%. |
|---|---|---|---|---|---|
| Acharya et al. 2012 [73] | Texture features to determine thyroid nodule malignancy. | • GLCM: $CON$, $H$, $HOM$ <br>• DWT | 5 (homogeneity, entropy, contrast, D2, D1) | AdaBoost with <br>• C4_5 configuration <br>• Perceptron configuration <br>• Pocket configuration <br>• Stump | The AdaBoost with perceptron configuration performed the best with classification accuracy, sensitivity, specificity of 100% |

| Acharya et al. 2011 [74] | Based on the idea that texture indicates the histopathologic components of the thyroid nodules. | • GLCM: Symmetry ($SYM$), $H$, $HOM$<br>• DWT | 10 (homogeneity, entropy, symmetry, A2, H2, H1, V2, V1, D2, D1) | • K-NN<br>• PNN<br>• DT | K-NN:(Accuracy: 98.9%, Sensitivity: 98%, Specificity: 99.8%) |
|---|---|---|---|---|---|
| Acharya et al. 2012 [75] | Determining the risk of malignancy by detecting suspicious ultrasound features with texture methods. | • FD<br>• $LBP$<br>• Fourier Spectrum descriptor (FS)<br>• LTE | 16 (1 FD, 6 $LBP$, 1 FS, 8 LTE) | SVM:<br>• Linear<br>• Polynomial Order 1<br>• Polynomial Order 2<br>• RBF<br><br>Other classifiers:<br>• DT<br>• Fuzzy<br>• GMM<br>• K-NN<br>• NBC<br>• PNN | HRUS dataset: SVM and Fuzzy classifiers performed the best with classification accuracy, sensitivity, specificity and positive predictive value of 100%<br>CEUS dataset: GMM classifier (Accuracy: 98.1%, Sensitivity: 97.2%, Specificity: 98.9%, Positive predictive value: 98.9%) |

| Kale et al. 2012 [76] | texture-based tissue information exaction. | GLCM: $ACORR$, $CON$, $CORR$, $CP$, $CS$, $DISS$, $E$, $H$, $MP$ | 10 (1 FD, 6 $LBP$, 1 FS, 8 LTE) | Scaled conjugate gradient backpropagation training feed forward neutral network | Classified malignant and benign nodule with accuracy of 95.33% and 91.89% respectively. Overall, the accuracy of classifier was 94.11%. |
|---|---|---|---|---|---|
| Kale et al. 2013 [77] | Texture features as a way to increase the quantitative information from thyroid US images. | GLCM: $ACORR$, $CON$, $CORR$, $CP$, $CS$, $DISS$, $E$, $H$, $HOM$, $MP$ | 10 (1 FD, 6 $LBP$, 1 FS, 8 LTE) | Linear SVM | Classification accuracy of 82.39 ± 1.83% for 450 orientations. |
| Acharya et al. 2014 [78] | Using homogeneous and heterogeneous texture to characterize thyroid tissue. | GLCM, LTE, $LBP$, Fourier spectrum descriptors | GMM, SVM, K-NN, PNN, DT, Adaboost, Fuzzy Sugeno | Not reported | Not reported |
| Acharya et al. 2016 [31] | texture-based feature extraction to classify benign and malignant thyroid nodules. | Gabor filter | 30 | SVM, K-NN, Multilayer perceptron, DT | Accuracy: 94.3% with DT |

## 5. Discussion

US images are non-uniform, they differ in terms of feature orientation, feature scale, image resolution and grey level scaling [79, 80]. The orientation ambiguity cannot be fixed, because the transducer head is flexible, the patient and indeed the scanned tissue itself move. The problem of feature scale is tackled by specifying a ROI. However, the most difficult problem for texture features, from US images, is grey level scaling and image resolution, because run length and GLCM methods are sensitive to these parameters. In other words, the feature values change in accordance with both spatial and grey level scale. The exact relationship between scale changes and feature value changes is unexplored. There are scaling invariant methods in existence, but the resulting features are not discriminative enough for high quality CAD systems and, in many cases, the associated algorithms are computationally complex [81]. For example, Local Configuration Pattern (LCP) are rotation invariant and they provide complementary information to $LBP$ [82].

For texture algorithms, computational complexity is just equipment investment and computation time. In general, computational complexity of feature extraction algorithms impact on latency and cost [83]. The cost rises in accordance with efforts to keep the latency down. However, the performance of processing systems doubles every 18 months[2], hence keeping the computational complexity down is a weak research objective.

Classical machine learning systems, such as the ones used in current CAD systems, require careful engineering and expert knowledge in order to create feature extractors [84]. The texture algorithms extract feature information from the US images. Subsequently, the extracted information is fed to machine learning algorithms. While that process is straight forward in the online system, domain specific expertise is required to test and select the best performing algorithm combination with the design centric offline system. The process of selecting the algorithm combination is based on experience as well as on trial and error. The method of trial and error implies that the resulting CAD system might be sub-optimal. To be specific, during the design phase only a limited number of feature algorithms can be tested. Hence, there might be other algorithms which outperform the selected methods. For example, a designer might not be aware of the GLRLM feature extraction methods. That knowledge gap would have a big impact on the thyroid cancer classification example, presented in Section 2.5, because a GLRLM method ($LRE$) was the best of the tested methods.

Deep learning eliminates the requirement for domain specific expertise in feature extraction algorithms, because these methods are fed with raw data. In case of US based soft tissue cancer detection, the deep learning algorithms would be fed with unprocessed US images. On the positive side, it eliminates the feature extraction step and the associated ambiguities[3] [85]. On the negative side, the diagnosis process becomes very abstract. Throughout the design of the offline system, there are quality control measures to ensure traceability. That means, if something goes wrong, it is possible to trace back into the design process and locate the error. In contrast, deep learning is a one step process without continuous quality monitoring. Ultimately, the decision on whether or not to use deep learning algorithms will depend on their performance for well-known standard problems [86]. To be specific, if deep learning

---

[2]Moors law, verified by observations from 1975 onward.

[3]Feature testing and selection.

based CAD systems deliver higher diagnosis accuracy, when compared to traditional feature based methods, then the new methods will supersede the traditional algorithm structures.

## 5.1. Future work

The future direction of US imaging can be summed up in one word: *radiomics* [87]. The term refers to the automated extraction and analysis of high dimensional feature vectors [88]. These feature vectors, combined with other patient data form the input to sophisticated bioinformatics tools which help to improve diagnostic and predictive accuracy [89]. All processing is done in the digital domain with computer algorithms executed by microchips. The inherent cost effectiveness, speed and scalability of this technology helps to cope with an ever increasing amount of medical images [90]. The main idea behind radiomics is to interpret medical images as data and the interpretation of that data is left to machines [91]. The assumption is that, new image processing algorithms are able to extract the salient features from the medical images which are the hidden signatures of the diseases. The postulated benefits focus on the strong points of computing technology. However, these methods are inflexible and therefore they fail to accommodate errors in the input data. In other words, radiomics proposes to replace or at least to diminish the role of the human brain, which has a negative impact on both safety and reliability of disease diagnosis. This poses considerable design challenges, which goes beyond 'good' engineering practice [92, 93]. Radiomics systems must be safe, reliable and functional [92]. The design process must ensure that systemic errors are minimized [94]. Errors may be caused by operator mistakes. The widespread deployment of CAD systems will depend on trust which is closely linked to justifications given for claims of reliability and system safety [95].

## 6. Conclusion

In this paper, we reviewed US texture features for soft tissue cancer detection. The study focused on thyroid, breast, ovarian, liver and prostate cancers. The texture feature extraction algorithms were introduced in an example study on thyroid cancer. In our example, the $LRE$ feature outperformed rest of the algorithms. However, the result is not representative, as it depends on the type of cancer detection, and on the type of imaging system used. These texture features are widely used in the development of CAD systems. Therefore, the CAD system must address the need for accurate and cost effective soft tissue cancer diagnosis.

During the review, we found that texture-based features for US image classification is an important topic, because these techniques extract useful information. However, these techniques need to be used in conjunction with other features, such as HOS, DWT and statistical features. In future, deep algorithms can be used to extract the abstract information contained in US images, which may improve the performance of US based cancer detection.

## 7. Acknowledgement

## 8. References

[1] R. L. Siegel, K. D. Miller, A. Jemal, Cancer statistics, 2015, CA: a cancer journal for clinicians 65 (1) (2015) 5–29.

[2] L. Rahib, B. D. Smith, R. Aizenberg, A. B. Rosenzweig, J. M. Fleshman, L. M. Matrisian, Projecting cancer incidence and deaths to 2030: the unexpected burden of thyroid, liver, and pancreas cancers in the united states, Cancer research 74 (11) (2014) 2913–2921.

[3] R. Siegel, A. Jemal, Cancer facts & figures 2015, American Cancer Society. Cancer Facts & Figures.

[4] D. Schottenfeld, Cancer epidemiology and prevention, Oxford University Press, 2006.

[5] P. Buell, J. E. Dunn, Cancer mortality among japanese issei and nisei of california, Cancer 18 (5) (1965) 656–664.

[6] U. R. Acharya, O. Faust, S. V. Sree, F. Molinari, L. Saba, A. Nicolaides, J. S. Suri, An accurate and generalized approach to plaque characterization in 346 carotid ultrasound scans, IEEE transactions on instrumentation and measurement 61 (4) (2012) 1045–1053.

[7] U. R. Acharya, O. Faust, F. Molinari, S. V. Sree, S. P. Junnarkar, V. Sudarshan, Ultrasound-based tissue characterization and classification of fatty liver disease: A screening and diagnostic paradigm, Knowledge-Based Systems 75 (2015) 66–77.

[8] R. U. Acharya, O. Faust, A. Alvin, S. V. Sree, F. Molinari, L. Saba, A. Nicolaides, J. S. Suri, Symptomatic vs. asymptomatic plaque classification in carotid ultrasound, Journal of medical systems 36 (3) (2012) 1861–1871.

[9] O. Faust, U. R. Acharya, V. K. Sudarshan, R. San Tan, C. H. Yeong, F. Molinari, K. H. Ng, Computer aided diagnosis of coronary artery disease, myocardial infarction and carotid atherosclerosis using ultrasound images: A review, Physica Medica 33 (2017) 1–15.

[10] P. G. Newman, G. S. Rozycki, The history of ultrasound, Surgical clinics of north America 78 (2) (1998) 179–195.

[11] J. L. Kendall, S. R. Hoffenberg, R. S. Smith, History of emergency and critical care ultrasound: the evolution of a new imaging paradigm, Critical care medicine 35 (5) (2007) S126–S130.

[12] C.-h. Chen, L.-F. Pau, P. S.-p. Wang, Handbook of pattern recognition and computer vision, Vol. 2, World Scientific, 1993.

[13] M. Bevk, I. Kononenko, A statistical approach to texture description of medical images: a preliminary study, in: Computer-Based Medical Systems, 2002.(CBMS 2002). Proceedings of the 15th IEEE Symposium on, IEEE, 2002, pp. 239–244.

[14] F. L. Lizzi, M. Greenebaum, E. J. Feleppa, M. Elbaum, D. J. Coleman, Theoretical framework for spectrum analysis in ultrasonic tissue characterization, The Journal of the Acoustical Society of America 73 (4) (1983) 1366–1373.

[15] W.-J. Wu, W. K. Moon, Ultrasound breast tumor image computer-aided diagnosis with texture and morphological features, Academic radiology 15 (7) (2008) 873–880.

[16] O. Faust, U. R. Acharya, E. Ng, T. J. Hong, W. Yu, Application of infrared thermography in computer aided diagnosis, Infrared Physics & Technology 66 (2014) 160–175.

[17] U. R. Acharya, O. Faust, N. A. Kadri, J. S. Suri, W. Yu, Automated identification of normal and diabetes heart rate signals using nonlinear measures, Computers in biology and medicine 43 (10) (2013) 1523–1529.

[18] U. R. Acharya, S. V. Sree, M. M. R. Krishnan, F. Molinari, L. Saba, S. Y. S. Ho, A. T. Ahuja, S. C. Ho, A. Nicolaides, J. S. Suri, Atherosclerotic risk stratification strategy for carotid arteries using texture-based features, Ultrasound in medicine & biology 38 (6) (2012) 899–915.

[19] D. K. Somwanshi, A. K. Yadav, R. Roy, et al., Medical images texture analysis: A review, in: Computer, Communications and Electronics (Comptelix), 2017 International Conference on, IEEE, 2017, pp. 436–441.

[20] A. Jalalian, S. B. Mashohor, H. R. Mahmud, M. I. B. Saripan, A. R. B. Ramli, B. Karasfi, Computer-aided detection/diagnosis of breast cancer in mammography and ultrasound: a review, Clinical imaging 37 (3) (2013) 420–426.

[21] M. L. Cher, K. V. Honn, A. Raz, Prostate cancer: new horizons in research and treatment, Springer, 2002.

[22] H. Zhao, Q. Zhu, Z. Wang, Detection of prostate cancer with three-dimensional transrectal ultrasound: correlation with biopsy results, The British journal of radiology 85 (1014) (2012) 714–719.

[23] S. A. Curley, Liver cancer, Springer Science & Business Media, 1998.

[24] J. Virmani, V. Kumar, N. Kalra, N. Khandelwal, Neural network ensemble based cad system for focal liver lesions from b-mode ultrasound, Journal of digital imaging 27 (4) (2014) 520–537.

[25] E. Banks, J. Bartlett, Ovarian cancer: Methods and protocols (2000).

[26] V. W. Chen, B. Ruiz, J. L. Killeen, T. R. Coté, X. C. Wu, C. N. Correa, H. L. Howe, Pathology and classification of ovarian tumors, Cancer 97 (S10) (2003) 2631–2642.

[27] L. Wartofsky, D. Van Nostrand, Thyroid cancer: a comprehensive guide to clinical management, Springer, 2016.

[28] D. Koundal, S. Gupta, S. Singh, Computer-aided diagnosis of thyroid nodule: a review, International Journal of Computer Science and Engineering Survey 3 (4) (2012) 67.

[29] T. L. Szabo, Diagnostic ultrasound imaging: inside out, Academic Press, 2004.

[30] J. Reid, The measurement of scattering, Tissue Characterization with Ultrasound (1986) 81–114.

[31] U. R. Acharya, P. Chowriappa, H. Fujita, S. Bhat, S. Dua, J. E. Koh, L. Eugene, P. Kongmebhol, K. Ng, Thyroid lesion classification in 242 patient population using gabor transform features from high resolution ultrasound images, Knowledge-Based Systems.

[32] J. F. Box, Guinness, gosset, fisher, and small samples, Statistical science (1987) 45–52.

[33] B. Shneiderman, M. Wattenberg, Ordered treemap layouts, in: Proceedings of the IEEE Symposium on Information Visualization 2001, Vol. 73078, 2001, pp. 1–6.

[34] K. Gurney, An introduction to neural networks, CRC press, 1997.

[35] I. Steinwart, A. Christmann, Support vector machines, Springer Science & Business Media, 2008.

[36] L. Rokach, O. Maimon, Data mining with decision trees: theory and applications, World scientific, 2014.

[37] M. E. Tarter, M. D. Lock, Model-free curve estimation, Vol. 56, CRC Press, 1993.

[38] S. Thirumuruganathan, A detailed introduction to k-nearest neighbor (knn) algorithm, Retrieved March 20 (2010) 2012.

[39] D. F. Specht, Probabilistic neural networks, Neural networks 3 (1) (1990) 109–118.

[40] I. Rish, An empirical study of the naive bayes classifier, in: IJCAI 2001 workshop on empirical methods in artificial intelligence, Vol. 3, IBM New York, 2001, pp. 41–46.

[41] D. L. James, R. Miikkulainen, Sardnet: A self-organizing feature map for sequences, Advances in neural information processing systems 7 (1995) 577.

[42] F. Rosenblatt, Principles of neurodynamics. perceptrons and the theory of brain mechanisms, Tech. rep., DTIC Document (1961).

[43] S. Haykin, N. Network, A comprehensive foundation, Neural Networks 2 (2004) (2004) 41.

[44] Y.-L. Huang, D.-R. Chen, Y.-K. Liu, Breast cancer diagnosis using image retrieval for different ultrasonic systems, in: Image Processing, 2004. ICIP'04. 2004 International Conference on, Vol. 5, IEEE, 2004, pp. 2957–2960.

[45] Y.-L. Huang, S.-H. Lin, D.-R. Chen, Computer-aided diagnosis applied to 3-d us of solid breast nodules by using principal component analysis and image retrieval, in: 2005 IEEE Engineering in Medicine and Biology 27th Annual Conference, IEEE, 2006, pp. 1802–1805.

[46] Y.-L. Huang, K.-L. Wang, D.-R. Chen, Diagnosis of breast tumors with ultrasonic texture analysis using support vector machines, Neural Computing & Applications 15 (2) (2006) 164–169.

[47] D.-R. Chen, W.-J. Kuo, R.-F. Chang, W. K. Moon, C. C. Lee, Use of the bootstrap technique with small training sets for computer-aided diagnosis in breast ultrasound, Ultrasound in medicine & biology 28 (7) (2002) 897–902.

[48] R.-F. Chang, W.-J. Wu, W. K. Moon, D.-R. Chen, Improvement in breast tumor discrimination by support vector machines and speckle-emphasis texture analysis, Ultrasound in medicine & biology 29 (5) (2003) 679–686.

[49] B. S. Garra, B. H. Krasner, S. C. Horii, S. Ascher, S. K. Mun, R. K. Zeman, Improving the distinction between benign and malignant breast lesions: the value of sonographic texture analysis, Ultrasonic imaging 15 (4) (1993) 267–285.

[50] X. Shi, H. Cheng, L. Hu, Mass detection and classification in breast ultrasound images using fuzzy svm., in: JCIS, 2006, pp. 1–4.

[51] W. Gómez, W. Pereira, A. F. C. Infantosi, Analysis of co-occurrence texture statistics as a function of gray-level quantization for classifying breast ultrasound, IEEE transactions on medical imaging 31 (10) (2012) 1889–1899.

[52] U. Scheipers, A. Lorenz, A. Pesavento, H. Ermert, H.-J. Sommerfeld, M. Garcia-Schurmann, K. Kuhne, T. Senge, S. Philippou, Ultrasonic multifeature tissue characterization for the early detection of prostate cancer, in: Ultrasonics Symposium, 2001 IEEE, Vol. 2, IEEE, 2001, pp. 1265–1268.

[53] W. D. Richard, C. G. Keen, Automated texture-based segmentation of ultrasound images of the prostate, Computerized Medical Imaging and Graphics 20 (3) (1996) 131–140.

[54] M. M. Mohamed, T. K. Abdel-Galil, E. F. El-saadany, A. Fenster, D. B. Downey, K. Rizkalla, Prostate cancer diagnosis based on gabor filter texture segmentation of ultrasound image, in: Electrical and Computer Engineering, 2003. IEEE CCECE 2003. Canadian Conference on, Vol. 3, IEEE, 2003, pp. 1485–1488.

[55] O. Basset, Z. Sun, J. L. Mestas, G. Gimenez, Texture analysis of ultrasonic images of the prostate by means of co-occurrence matrices, Ultrasonic Imaging 15 (3) (1993) 218–237.

[56] S. M. Han, H. J. Lee, J. Y. Choi, Computer-aided prostate cancer detection using texture features and clinical features in ultrasound image, Journal of digital imaging 21 (1) (2008) 121–133.

[57] A. L. Huynen, R. J. B. Giesen, J. J. M. C. H. De La Rosette, R. G. Aarnink, F. M. J. Debruyne, H. Wijkstra, Analysis of ultrasonographic prostate images for the detection of prostatic carcinoma: the automated urologic diagnostic expert system, Ultrasound in medicine & biology 20 (1) (1994) 1–10.

[58] U. Scheipers, H. Ermert, H.-J. Sommerfeld, M. Garcia-Schürmann, T. Senge, S. Philippou, Ultrasonic multifeature tissue characterization for prostate diagnostics, Ultrasound in medicine & biology 29 (8) (2003) 1137–1149.

[59] S. Pavlopoulos, E. Kyriacou, D. Koutsouris, K. Blekas, A. Stafylopatis, P. Zoumpoulis, Fuzzy neural network-based texture analysis of ultrasonic images, Engineering in Medicine and Biology Magazine, IEEE 19 (1) (2000) 39–47.

[60] S. Poonguzhali, G. Ravindran, Automatic classification of focal lesions in ultrasound liver images using combined texture features, Information Technology Journal 7 (1) (2008) 205–209.

[61] G.-m. Xian, An identification method of malignant and benign liver tumors from ultrasonography based on glcm texture features and fuzzy svm, Expert Systems with Applications 37 (10) (2010) 6737–6741.

[62] U. R. Acharya, S. V. Sree, R. Ribeiro, G. Krishnamurthi, R. T. Marinho, J. Sanches, J. S. Suri, Data mining framework for fatty liver disease classification in ultrasound: a hybrid feature extraction paradigm, Medical physics 39 (7) (2012) 4255–4264.

[63] M. Singh, S. Singh, S. Gupta, An information fusion based method for liver classification using texture analysis of ultrasound images, Information Fusion 19 (2014) 91–96.

[64] K. R. Krishnan, R. Sudhakar, Automatic classification of liver diseases from ultrasound images using glrlm texture features, in: Soft Computing Applications, Springer, 2013, pp. 611–624.

[65] U. R. Acharya, U. Raghavendra, H. Fujita, Y. Hagiwara, J. E. Koh, T. J. Hong, V. K. Sudarshan, A. Vijayananthan, C. H. Yeong, A. Gudigar, Automated characterization of fatty liver disease and cirrhosis using curvelet transform and entropy features extracted from ultrasound images, Computers in Biology and Medicine 79 (2016) 250–258.

[66] U. R. Acharya, H. Fujita, S. Bhat, U. Raghavendra, A. Gudigar, F. Molinari, A. Vijayananthan, K. H. Ng, Decision support system for fatty liver disease using gist descriptors extracted from ultrasound images, Information Fusion 29 (2016) 32–39.

[67] U. R. Acharya, L. Saba, F. Molinari, S. Guerriero, J. S. Suri, Ovarian tumor characterization and classification using ultrasound: A new online paradigm, in: Ovarian Neoplasm Imaging, Springer, 2013, pp. 413–423.

[68] U. R. Acharya, M. M. R. Krishnan, L. Saba, F. Molinari, S. Guerriero, J. S. Suri, Ovarian tumor characterization using 3d ultrasound, in: Ovarian Neoplasm Imaging, Springer, 2013, pp. 399–412.

[69] U. R. Acharya, S. V. Sree, S. Kulshreshtha, F. Molinari, J. E. W. Koh, L. Saba, J. S. Suri, Gynescan: an improved online paradigm for screening of ovarian cancer via tissue characterization, Technology in cancer research & treatment 13 (6) (2014) 529–539.

[70] S. Khazendar, A. Sayasneh, H. Al-Assam, H. Du, J. Kaijser, L. Ferrara, D. Timmerman, S. Jassim, T. Bourne, Automated characterisation of ultrasound images of ovarian tumours: the diagnostic accuracy of a support vector machine and image processing with a local binary pattern operator, Facts, views & vision in ObGyn 7 (1) (2015) 7.

[71] U. R. Acharya, F. Molinari, S. V. Sree, G. Swapna, L. Saba, S. Guerriero, J. S. Suri, Ovarian tissue characterization in ultrasound: a review, Technology in cancer research & treatment 14 (3) (2015) 251–261.

[72] C.-Y. Chang, S.-J. Chen, M.-F. Tsai, Application of support-vector-machine-based method for feature selection and classification of thyroid nodules in ultrasound images, Pattern recognition 43 (10) (2010) 3494–3506.

[73] U. R. Acharya, O. Faust, S. V. Sree, F. Molinari, J. S. Suri, Thyroscreen system: high resolution ultrasound thyroid image characterization into benign and malignant classes using novel combination of texture and discrete wavelet transform, Computer methods and programs in biomedicine 107 (2) (2012) 233–241.

[74] U. Acharya, O. Faust, S. V. Sree, F. Molinari, R. Garberoglio, J. Suri, Cost-effective and non-invasive automated benign & malignant thyroid lesion classification in 3d contrast-enhanced ultrasound using combination of wavelets and textures: a class of thyroscan algorithms, Technology in cancer research & treatment 10 (4) (2011) 371–380.

[75] U. R. Acharya, S. V. Sree, M. M. R. Krishnan, F. Molinari, R. Garberoglio, J. S. Suri, Non-invasive automated 3d thyroid lesion classification in ultrasound: a class of thyroscan systems, Ultrasonics 52 (4) (2012) 508–520.

[76] S. D. Kale, K. M. Punwatkar, Y. Pusad, Texture analysis of thyroid ultrasound images for diagnosis of benign and malignant nodule using scaled conjugate gradient back-propagation training neural network, IJCEM International Journal of Computational Engineering & Management 16 (6).

[77] S. D. Kale, K. M. Punwatkar, Texture analysis of ultrasound medical images for diagnosis of thyroid nodule using support vector machine, International Journal of Computer Science and Mobile Computing 2 (2013) 71–77.

[78] U. R. Acharya, G. Swapna, S. V. Sree, F. Molinari, S. Gupta, R. H. Bardales, A. Witkowska, J. S. Suri, A review on ultrasound-based thyroid cancer tissue characterization and automated classification, Technology in cancer research & treatment 13 (4) (2014) 289–301.

[79] U. R. Acharya, O. Faust, S. V. Sree, A. P. C. Alvin, G. Krishnamurthi, J. Sanches, J. S. Suri, Atheromatic: Symptomatic vs. asymptomatic classification of carotid ultrasound plaque using a combination of hos, dwt & texture, in: 2011 Annual International Conference of the IEEE Engineering in Medicine and Biology Society, IEEE, 2011, pp. 4489–4492.

[80] U. R. Acharya, O. Faust, A. Alvin, G. Krishnamurthi, J. C. Seabra, J. Sanches, J. S. Suri, Understanding symptomatology of atherosclerotic plaque by image-based tissue characterization, Computer methods and programs in biomedicine 110 (1) (2013) 66–75.

[81] L. Wang, G. Healey, Using zernike moments for the illumination and geometry invariant classification of multispectral texture, Image Processing, IEEE Transactions on 7 (2) (1998) 196–203.

[82] Y. Guo, G. Zhao, M. Pietikäinen, Texture classification using a linear configuration model based descriptor, BMVC (2011) 1–10.

[83] O. Faust, W. Yu, U. R. Acharya, The role of real-time in biomedical science: A meta-analysis on computational complexity, delay and speedup, Computers in biology and medicine 58 (2015) 73–84.

[84] Y. LeCun, Y. Bengio, G. Hinton, Deep learning, Nature 521 (7553) (2015) 436–444.

[85] J. Schmidhuber, Deep learning in neural networks: An overview, Neural Networks 61 (2015) 85–117.

[86] B. Chandrasekaran, S. Mittal, Deep versus compiled knowledge approaches to diagnostic problem-solving, International Journal of Man-Machine Studies 19 (5) (1983) 425–436.

[87] V. Parekh, M. A. Jacobs, Radiomics: a new application from established techniques, Expert Review of Precision Medicine and Drug Development 1 (2) (2016) 207–226.

[88] V. Kumar, Y. Gu, S. Basu, A. Berglund, S. A. Eschrich, M. B. Schabath, K. Forster, H. J. Aerts, A. Dekker, D. Fenstermacher, Radiomics: the process and the challenges, Magnetic resonance imaging 30 (9) (2012) 1234–1248.

[89] C. Parmar, E. R. Velazquez, R. Leijenaar, M. Jermoumi, S. Carvalho, R. H. Mak, S. Mitra, B. U. Shankar, R. Kikinis, B. Haibe-Kains, Robust radiomics feature quantification using semiautomatic volumetric segmentation, PloS one 9 (7) (2014) e102107.

[90] K. Ng, O. Faust, V. Sudarshan, S. Chattopadhyay, Data overloading in medical imaging: Emerging issues, challenges and opportunities in efficient data management, Journal of Medical Imaging and Health Informatics 5 (4) (2015) 755–764.

[91] R. J. Gillies, P. E. Kinahan, H. Hricak, Radiomics: images are more than pictures, they are data, Radiology 278 (2) (2015) 563–577.

[92] O. Faust, U. R. Acharya, T. Tamura, Formal design methods for reliable computer-aided diagnosis: a review, IEEE reviews in biomedical engineering 5 (2012) 15–28.

[93] O. Faust, R. Acharya, B. H. Sputh, L. C. Min, Systems engineering principles for the design of biomedical signal processing systems, Computer methods and programs in biomedicine 102 (3) (2011) 267–276.

[94] O. Faust, B. H. Sputh, U. Acharya, A. R. Allen, A pervasive design strategy for distributed health care systems, Open Medical Imaging Journal 2 (2008) 58–69.

[95] Z. Song, Z. Ji, J.-G. Ma, B. Sputh, U. R. Acharya, O. Faust, A systematic approach to embedded biomedical decision making, Computer methods and programs in biomedicine 108 (2) (2012) 656–664.

## Appendix A. Texture Feature Results

Table A.7: Performance measures for the individual texture features.

| | Benign | | Malignant | | | |
|---|---|---|---|---|---|---|
| | Mean | SD | Mean | SD | $p$-value | $t$-value |
| $LRE$ | 1.98E+01 | 1.86E+00 | 1.81E+01 | 1.92E+00 | 0.0011 | 3.4354 |
| $SVAR$ | 4.24E+01 | 7.64E+00 | 3.59E+01 | 7.20E+00 | 0.0015 | 3.3356 |
| $ACORR$ | 1.87E+01 | 3.19E+00 | 1.61E+01 | 2.97E+00 | 0.0019 | 3.2621 |
| $SA$ | 7.77E+00 | 8.78E-01 | 7.08E+00 | 7.74E-01 | 0.0024 | 3.1786 |
| $SKE$ | 3.98E-01 | 2.66E-01 | 5.79E-01 | 2.96E-01 | 0.0178 | 2.4424 |
| $SRE$ | 1.22E-01 | 2.99E-02 | 1.39E-01 | 2.49E-02 | 0.0209 | 2.3790 |
| $LRLGE$ | 8.95E+00 | 1.57E+00 | 8.04E+00 | 1.60E+00 | 0.0339 | 2.1747 |
| $CS$ | 2.16E+01 | 1.61E+01 | 2.95E+01 | 1.17E+01 | 0.0356 | 2.1581 |
| $KUR$ | 2.38E+00 | 3.17E-01 | 2.62E+00 | 5.18E-01 | 0.0394 | 2.1197 |
| $MP$ | 1.57E-01 | 7.91E-02 | 1.96E-01 | 6.29E-02 | 0.0454 | 2.0494 |
| $HGRE$ | 4.06E+01 | 4.01E+01 | 6.32E+01 | 5.23E+01 | 0.0709 | 1.8436 |
| LTE5 | 1.43E+07 | 2.81E+06 | 1.30E+07 | 2.77E+06 | 0.0737 | 1.8226 |
| $SENT$ | 2.52E+00 | 1.46E-01 | 2.46E+00 | 1.30E-01 | 0.0767 | 1.8039 |
| $D$ | 2.38E+00 | 3.30E-02 | 2.36E+00 | 3.61E-02 | 0.0791 | 1.7887 |
| $H$ | 2.90E+00 | 2.17E-01 | 2.80E+00 | 2.10E-01 | 0.0888 | 1.7319 |
| $SRLGE$ | 4.81E-02 | 1.05E-02 | 5.25E-02 | 9.09E-03 | 0.0968 | 1.6895 |
| $SRHGE$ | 1.50E+01 | 3.59E+01 | 2.95E+01 | 3.76E+01 | 0.1374 | 1.5072 |
| $RP$ | 2.47E+01 | 4.16E+00 | 2.31E+01 | 4.53E+00 | 0.1433 | 1.4844 |
| LTE1 | 4.82E+06 | 2.72E+06 | 3.82E+06 | 2.45E+06 | 0.1463 | 1.4733 |
| $HOM$ | 8.14E-01 | 3.40E-02 | 8.27E-01 | 3.42E-02 | 0.1549 | 1.4418 |
| $DISS$ | 4.04E-01 | 8.14E-02 | 3.74E-01 | 8.05E-02 | 0.1630 | 1.4135 |
| LBP Entropy 162 | 3.46E+00 | 9.41E-02 | 3.42E+00 | 1.19E-01 | 0.1685 | 1.3959 |
| $ICM1$ | -5.14E-01 | 5.13E-02 | -5.33E-01 | 5.29E-02 | 0.1882 | 1.3323 |
| $DVAR$ | 5.26E-01 | 1.37E-01 | 4.79E-01 | 1.32E-01 | 0.1909 | 1.3239 |
| $CON$ | 5.26E-01 | 1.37E-01 | 4.79E-01 | 1.32E-01 | 0.1909 | 1.3239 |
| $DENT$ | 7.62E-01 | 9.13E-02 | 7.30E-01 | 9.44E-02 | 0.1926 | 1.3189 |
| LTE6 | 2.69E+05 | 1.53E+05 | 2.21E+05 | 1.34E+05 | 0.2157 | 1.2525 |
| $E$ | 8.22E-02 | 4.14E-02 | 9.36E-02 | 2.84E-02 | 0.2273 | 1.2225 |

| | | | | | | |
|---|---|---|---|---|---|---|
| LTE2 | 7.74E+05 | 5.60E+05 | 6.10E+05 | 5.36E+05 | 0.2590 | 1.1405 |
| *GLNU* | 2.49E+04 | 7.87E+03 | 2.25E+04 | 8.09E+03 | 0.2590 | 1.1403 |
| *RLNU* | 1.70E+04 | 2.74E+03 | 1.61E+04 | 3.27E+03 | 0.2793 | 1.0929 |
| *LGRE* | 4.39E-01 | 6.34E-02 | 4.22E-01 | 6.90E-02 | 0.3429 | 0.9566 |
| LTE20 | 2.24E+06 | 8.34E+05 | 2.52E+06 | 1.32E+06 | 0.3476 | 0.9486 |
| LBP Entropy 243 | 3.45E+00 | 1.81E-01 | 3.40E+00 | 2.58E-01 | 0.3523 | 0.9388 |
| LBP Energy 81 | 1.57E-01 | 2.14E-02 | 1.52E-01 | 2.23E-02 | 0.3629 | 0.9174 |
| LTE7 | 4.40E+04 | 3.11E+04 | 3.68E+04 | 2.93E+04 | 0.3660 | 0.9114 |
| LTE3 | 4.80E+05 | 3.97E+05 | 3.88E+05 | 3.87E+05 | 0.3747 | 0.8949 |
| LBP Energy 162 | 1.56E-01 | 1.90E-02 | 1.61E-01 | 2.92E-02 | 0.4645 | 0.7374 |
| LTE11 | 7.22E+04 | 3.94E+04 | 6.46E+04 | 4.03E+04 | 0.4686 | 0.7297 |
| LBP Entropy 81 | 2.96E+00 | 1.08E-01 | 2.98E+00 | 1.25E-01 | 0.4929 | 0.6903 |
| LTE4 | 1.30E+06 | 1.19E+06 | 1.09E+06 | 1.14E+06 | 0.5026 | 0.6747 |
| LTE8 | 2.07E+04 | 1.53E+04 | 1.82E+04 | 1.58E+04 | 0.5399 | 0.6168 |
| *ICM2* | 9.25E-01 | 1.33E-02 | 9.27E-01 | 1.27E-02 | 0.5583 | 0.5889 |
| LBP Energy 243 | 2.14E-01 | 3.43E-02 | 2.21E-01 | 5.17E-02 | 0.5606 | 0.5860 |
| LTE12 | 1.33E+04 | 8.83E+03 | 1.20E+04 | 9.30E+03 | 0.6002 | 0.5271 |
| LTE21 | 8.22E+04 | 4.14E+04 | 8.97E+04 | 6.59E+04 | 0.6097 | 0.5139 |
| LTE10 | 2.48E+06 | 6.32E+05 | 2.39E+06 | 6.97E+05 | 0.6169 | 0.5031 |
| *LRHGE* | 5.64E+02 | 3.36E+02 | 6.00E+02 | 3.14E+02 | 0.6787 | 0.4165 |
| LTE13 | 6.97E+03 | 5.15E+03 | 6.43E+03 | 5.50E+03 | 0.6994 | 0.3881 |
| LTE22 | 2.14E+04 | 1.29E+04 | 2.30E+04 | 1.75E+04 | 0.7037 | 0.3824 |
| LTE15 | 1.27E+06 | 3.96E+05 | 1.31E+06 | 5.76E+05 | 0.7466 | 0.3249 |
| LTE9 | 4.26E+04 | 4.04E+04 | 3.89E+04 | 4.72E+04 | 0.7498 | 0.3205 |
| LTE14 | 1.62E+04 | 1.65E+04 | 1.51E+04 | 1.78E+04 | 0.8164 | 0.2333 |
| LTE24 | 7.47E+04 | 7.51E+04 | 7.95E+04 | 8.17E+04 | 0.8182 | 0.2309 |
| LTE19 | 1.74E+04 | 1.89E+04 | 1.66E+04 | 1.81E+04 | 0.8678 | 0.1672 |
| LTE23 | 1.82E+04 | 1.41E+04 | 1.88E+04 | 1.55E+04 | 0.8824 | 0.1486 |
| LTE18 | 5.89E+03 | 4.47E+03 | 5.73E+03 | 4.78E+03 | 0.8998 | 0.1265 |
| *VAR* | 5.83E-02 | 9.38E-03 | 5.82E-02 | 1.16E-02 | 0.9685 | 0.0396 |
| LTE17 | 9.27E+03 | 5.76E+03 | 9.32E+03 | 7.24E+03 | 0.9726 | 0.0345 |
| LTE16 | 4.41E+04 | 2.29E+04 | 4.42E+04 | 3.07E+04 | 0.9861 | 0.0175 |